Three-Dimensional Plume Simulation of Multi-Channel Hall Effect Thruster

IEPC-2011-089

Presented at the 32nd International Electric Propulsion Conference,
Wiesbaden • Germany
September 11 – 15, 2011

F. Taccogna[1] and P. Minelli[2]
Istituto di Metodologie Inorganiche e di Plasmi, Consiglio Nazionale delle Ricerche, Bari, 70126, Italy

G. Coduti[3], D. Pagano[4] and F. Scortecci[5]
AEROSPAZIO Tecnologie S.r.l., Rapolano Terme, Siena, 53040, Italy

and

A. Garulli[6]
Dipartimento di Ingegneria dell'Informazione, Università di Siena, Siena, 53100, Italy

Abstract: A three-dimensional hybrid Particle-in-Cell model of the plume emitted by a four-channel Hall thruster configuration has been developed. Results show the presence of a potential well in the central region close to the exit plane of the configuration and the important role of charge exchange ion-neutral collisions, and geometrical effects on the ion energy spectra in the plume.

Nomenclature

A	=	fitting parameter in the charge exchange methodology collision
e	=	elementary charge = $1.602189\text{x}10^{-19}$ C
E	=	electric field / energy
g	=	relative velocity
k_B	=	Boltzmann constant = $1.380662\text{x}10^{-23}$
L	=	length of the simulation domain
$\dot{m}$	=	mass flow rate
m	=	electron mass = $9.11\text{x}10^{-31}$ Kg
M	=	ion mass (Xe) = $2.18\text{x}10^{-25}$ Kg
n	=	density
r	=	radial direction
r_{in}	=	inner radius of the channel
r_{out}	=	outer radius of the channel
$rand$	=	random number $\in[0,1]$

[1] Researcher, IMIP-CNR, francesco.taccogna@ba.imip.cnr.it.
[2] Researcher, IMIP-CNR, pierpaolo.minelli@ba.imip.cnr.it.
[3] AEROSPAZIO Tecnologie S.r.l., giovanni.coduti@aerospazio.com.
[4] AEROSPAZIO Tecnologie S.r.l., damiano.pagano@aerospazio.com.
[5] AEROSPAZIO Tecnologie S.r.l., fscortecci@aerospazio.com.
[6] Full Professor, Dipartimento di Ingegneria dell'Informazione, Università di Siena, garulli@ing.unisi.it.

z	=	axial direction
α_d	=	polarizability
γ	=	adiabatic exponent
Δt	=	time-step
ε_0	=	vacuum permittivity = $8.854188\text{x}10^{-12}$ F/m
η	=	ionization efficiency
θ	=	zenital angle
μ	=	reduced mass
ν	=	collisional frequency
π	=	pi-greek = 3.1415926536
ρ	=	charge density
σ	=	cross section
ϕ	=	electric potential
χ	=	deflection angle

I. Introduction

FUTURE applications of electric propulsion foresee high power regimes for Hall effect thrusters. The obvious answer to this request is to design a single thruster capable of operating at high power levels [1]. However, this monolithic approach may results in problems connected with testing and qualification due to the lack of ground facilities capable of maintaining adequate test pressures while supporting the high mass flow rate required.

A better solution can be clustering several lower power Hall thrusters [2-3]. Although a cluster of thrusters may have a slightly lower efficiency and higher dry mass in respect with similarly powered monolithic thrusters, this approach presents some important advantages. In fact, a cluster provides propulsion system redundancy and the ability to vary the system power while allowing the thrusters in use to operate at their peak efficiency. Clusters also provide the ability to control the direction of the thrust vector without relying on thruster pointing mechanism exploiting the capacity of generating torques about the centre of mass by simply turning off one or more thrusters. On the other hand, it is possible to counteract the parasitic torques due to the variation of the centre of gravity of the spacecraft determined by thermal deformations and propellant consumption.

A solution that mitigates the increase of the cluster mass, keeping its advantages, is represented by multi-channel thrusters [4]. These devices may include two, three or four discharge and acceleration channels, arranged in such a way to minimize the mass of the shared magnetic circuit and structure. Moreover, the different channels share the cathode [5], the xenon feed systems and the electrical harness. Therefore, the mass penalty compared to a single thruster of equivalent power is significantly lower than that of a conventional cluster of thrusters.
Each discharge can be throttled independently in order to control the angular deviation of the resultant thrust vector [6]: because of the thrust is substantially proportional to discharge current and mass flow rate over a large range about the nominal operating point, the individual thrust generated by each channel can be governed by modifying the mass flow rate keeping constant the common magnetic field and anode voltage.

Plasma plume flows from a single thruster have been simulated widely with particle methods [7,8]. These simulations adopt simplified axi-symmetric configurations and the plasma potential is usually solved by the simplest Boltzmann relation (isothermal approximation). There are several problems associated with these simplifications:
a) with more than one thrusters, plasma plume flows from different thrusters may interact with each other; consequently, the axial symmetry is not more valid;
b) there are some detailed near-field objects, such as thruster cathode-neutralizers;
c) the simple Boltzmann relation does not take into account the strong inhomogeneity in the electron temperature;
d) thrusters are usually tested in large vacuum chambers; the finite background pressure and chamber walls may have important effects on the plume flows.
In order to answer these questions, in this work we present a three-dimensional model of the dynamics of the plasma emitted from a configuration of four-channel SPT-40; each discharge has a power of 500 W (I_D=1 A, ϕ_D=500 V each one) for an overall power of 2 kW. The channels share the cathode neutralizer located in the center.

II. Numerical Model

The model consists of a hybrid particle-in-cell (PIC) method [9,10] and it represents an extension of previous two-dimensional axial-simmetric models [11,12]. Fig 1.a shows the simulation domain which consists of a cubic box of side L_x=L_y=L_z=2 m. The exit plane of the multi-channel thruster lie on the z=0 plane (Fig. 1.b). This allows the simulation of plume with any number of channels in operation, differently to others three-dimensional models

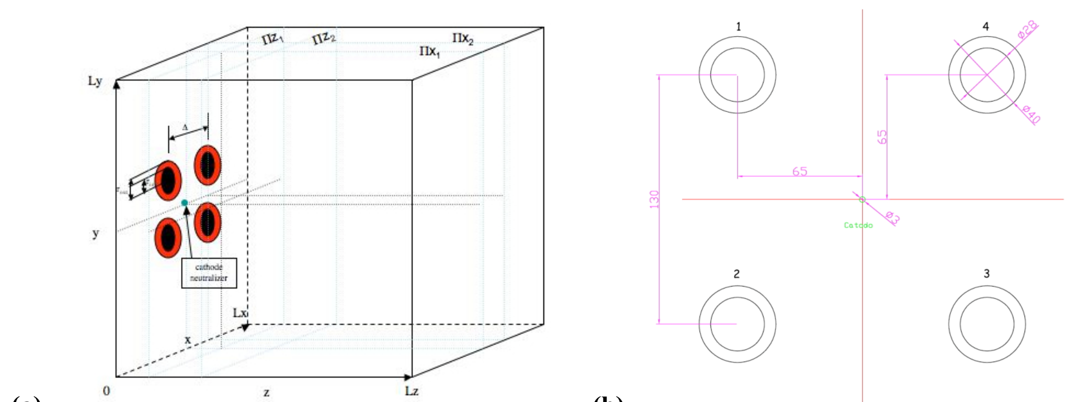

(a) **(b)**

Figure 1. (a) Simulation Domain and (b) sketch of the exit plane.

that simulate only one plume of the configuration [13] (the full plume field are obtained by reflections due to the symmetric configuration). Table I lists all the physical parameters of the system studied.

The problem can be considered as purely electrostatic. The magnetic field decays very rapidly outside the multichannel, already few millimetres from the exit plane, we can assume that electrons are un-magnetized. In addition, the ion time scale is much longer than the time the light takes to travel the entire computational region and then we can eliminate the electromagnetic waves. The electric field adapts instantly to the charge distribution in the system.

The electron time scale is much smaller than the ion one (490 times smaller in the case of xenon). This makes the fluid dynamics a plausible approach for the electrons. In particular, we have used the Boltzmann relation:

$$n_e(x,y,z) = n_0 \exp\left(\frac{q\phi(x,y,z)}{k_B T_e(x,y,z)}\right) \tag{1}$$

where the electron temperature is not homogeneous over the entire domain and it is calculated using the adiabatic relation:

$$T_e(x,y,z) = T_0\left(\frac{n_e(x,y,z)}{n_0}\right)^{\gamma-1} \tag{2}$$

Reference density n_0 and temperature T_0 have been chosen to correspond to experimental values.

The static background in which charged particles are injected is represented by unionized propellant, Xe atoms emitted by the multichannel configuration (the vacuum chamber effect can be easily added). Rather than distribute homogeneously neutrals in the simulation domain, we launched a Direct Simulation Monte Carlo [14] (DSMC) code of free flight of the neutral gas and we got a three-dimensional distribution of Xe density with their three velocity

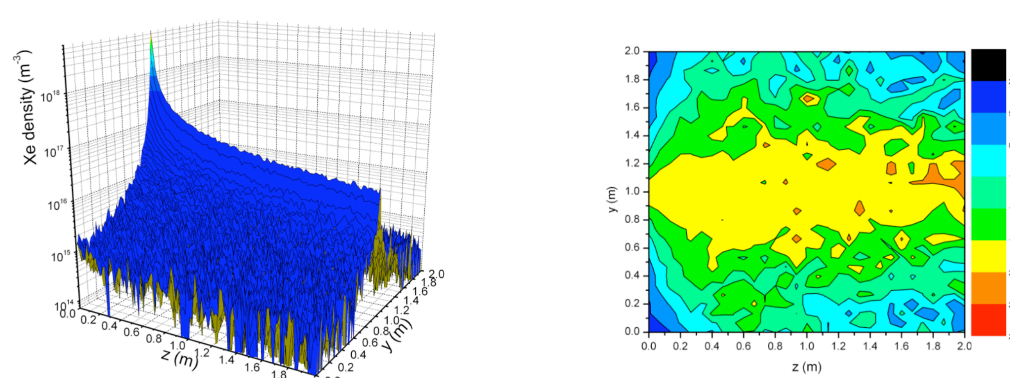

(a) **(b)**

Figure 2. Xe atom (a) density $n_{Xe}(m^{-3})$ and (b) axial velocity $v_{z,Xe}$ (ms^{-1}) in the plane Πx1.

components. The injection conditions are the following: an equivalent of $(1-\eta_i)\dot{m}$ is emitted from each channel, while $\dot{m}$ is emitted from the cathode neutralizer with a half-Maxwellian distribution (T_{Xe}=1000 K). These distributions (see Figs. 2 where Xe density and axial velocity in the plane Πx_1 are reported) have been used as input data for calculating ion-neutral collisions in the PIC model.

The sequence of computational code can be schematized as following:

1. Initialization: all variables that are generated and not updated during the various PIC cycles of the code.
2. Injection of particles: each channel injects the same number of macro-ions given by:

$$\Delta N_i = \frac{\eta_i \dot{m} \Delta t}{M_{Xe} w} \tag{3}$$

See Table II for the simulation parameters used. For each channel, the ions are injected according to a defined distribution of the radial distance *r* from the axis of the single channel (see Fig. 3.a) and a defined distribution of the zenital angle $\theta(r)$ (see Fig. 3.b), while the azimuthal angle is uniformly distributed between 0 and 360 degrees. These data have been determined through a fit of experimental measurements [15] of the ion current density taken at a distance of 4mm from the exit plane of an SPT-100. The module of the velocity $v=(2aq\Delta\phi/M_{Xe})^{1/2}$ will depend

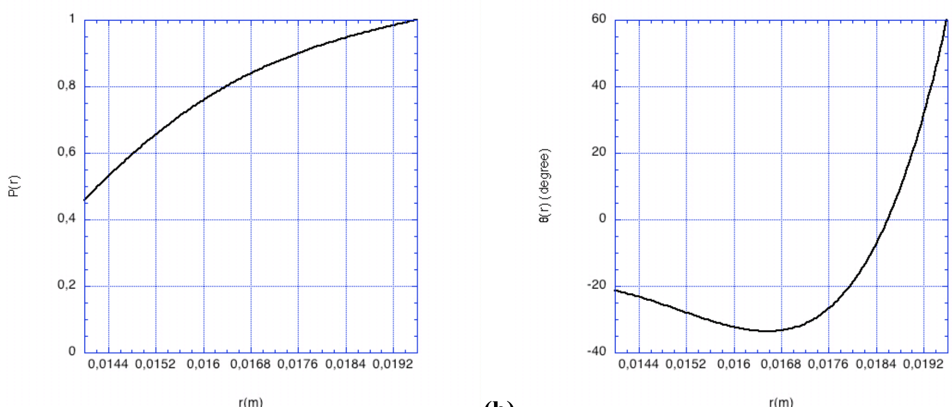

(a) **(b)**

Figure 3. Probability distribution function of radial position (r is respect to the axis of each channel) and zenital angle (in degree respect to the normal direction to the exit plane) of macro-ions injected.

on the speed of the emitted particle (a=1 for single ionized ions and a=2 for double ionized ions) given by the acceleration gained in the channel through the axial potential drop $\Delta\phi=\phi_D-\phi_{exit\ plane}$.

3. Deposition of the charge on the nodes of the grid, using factorized linear weight functions $P'(x,y,z)=P(x)P(y)P(z)$. The charge carried by particles is distributed on the closest grid points.
4. Solution of the electric field on the nodes of the grid: it represents the connection between the particle part (ionic component) and the fluid part (electronic component) of the code. With the Boltzmann relation, the Poisson equation takes the form of nonlinear differential elliptical equation:

$$\nabla^2\phi(x,y,z) + \frac{\rho_i(x,y,z)}{\varepsilon_0} - \frac{\rho_{e\infty}}{\varepsilon_0} e^{q\phi(x,y,z)/kT_e(x,y,z)} = 0 \tag{4}$$

It has been linearized and solved through the Newton-Raphson relaxation method [10], taking in consideration the following boundary conditions:

a) channel exit plane (red area in Fig. 1.a): $\phi_{exit\ plane}=2\phi_D/3$ (one third of the total drop is supposed to occur in the plume region);

b) surface thruster (black area in Figure 2): $\phi_{thruster}=\phi_{plasma}-k_BT_e/2$ V (where ϕ_{plasma} represents the value of the next mesh point in axial direction z); this condition corresponds to the sheath drop;

c) planes x=0 and $x=L_x$: $\partial\phi/\partial x$=0;

d) planes y=0 and y=L_y: $\partial\phi/\partial y$=0;
e) planes z=0 and z=L_z: $\partial\phi/\partial z$=0.

5. Interpolation of all the three electric field components on the particle positions using the same weight functions used in the step 3.

6. Integration of the equations of motion: we obtain the displacement and the variation of the three velocity components of the ion during the PIC time-step through the leap-frog method.

7. Treatment of ion-neutral collisions, according to on an attractiv

$$U(r) = -\frac{\alpha_d e^2}{2(4\pi\varepsilon_0)^2}\frac{1}{r^4} \quad (5)$$

where α_d is the Xenon polarizability. This assumption corresponds to a dipole-induced dipole interaction. The first step is to calculate the collision interval τ_c given, in the case of polarization potential, by

$$\tau_c = -\frac{2\varepsilon_0}{e\beta_\infty^2}\sqrt{\frac{\mu}{\alpha_d}}\frac{\ln(rand)}{n_N}. \quad (6)$$

If $\tau_c<\Delta t$, a random sample of the non-dimensional impact parameter and the azimuthal angle are given by the following distributions:

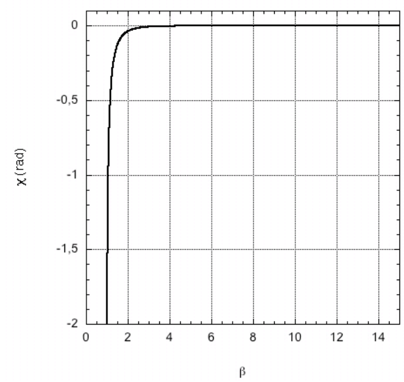

Figure 4. Deflection angle as a function of normilez impact parameter in the Nanbu-Kitatani model [16].

$$\beta = \frac{\beta_\infty}{\sqrt{rand}} \quad (7)$$

$$\varphi = 2\pi\, rand\,. \quad (8)$$

Next, we calculate the deflection angle according to the impact parameter (see Fig. 4). If $\beta>\beta_{cx}$ a momentum transfer collision (MX) occurs and the ion post-collisional velocity is calculated as

$$\mathbf{v}' = \mathbf{v} + \frac{1}{2}\left[\mathbf{g}(1-\cos\chi) + \mathbf{h}\sin\chi\right]. \quad (9.a)$$

If $\beta<\beta_{cx}=A(\mu g^2/2)^{1/4}$, a new ion appears with a probability of 0.5 (charge exchange collision, CX) and with a post-collisional velocity equal to

$$\mathbf{v}' = \mathbf{v}_N - \frac{1}{2}\left[\mathbf{g}(1-\cos\chi) + \mathbf{h}\sin\chi\right] \quad (9.b)$$

where

$$\begin{aligned} h_r &= (g_\theta^2 + g_z^2)^{1/2}\cos\varphi \\ h_\theta &= -\frac{g_\theta g_r \cos\varphi + g\, g_z \sin\varphi}{(g_\theta^2 + g_z^2)^{1/2}} \\ h_y &= -\frac{g_z g_r \cos\varphi - g\, g_\theta \sin\varphi}{(g_\theta^2 + g_z^2)^{1/2}} \end{aligned} \quad (9.c)$$

and the "virtual" target velocity $\boldsymbol{v}_N$ is taken from neutral DSMC code results.

Points ranging from 2 to 7 are cyclically repeated until convergence is reached.

Table I – The most important physical parameters representing the multi-channel configuration simulated.

Physical Parameter	**Value**
External radius r_{out} (m) of each channel	0.02
Internal radius r_{in} (m) of each channel	0.014
Center-to-center distance Δ (m)	0.13
Voltage discharge ϕ_D (V)	500
Ionization efficiency η_i	0.95
Anode mass flow rate $\dot{m}$ (mg/s) (for each channel)	1
Plume composition at the exit plane: Xe^+/Xe^{++}	0.9/0.1

Table II – The most important simulation parameters used in the code.

Simulation Parameter	**Value**
Time step Δt (s)	2×10^{-7}
Macroparticle weight w	1×10^{8}
Domain size L_xxL_yxL_z (m^3)	8
Mesh points N_xxN_yxN_z	120x120x120
Cell volume ΔxxΔyxΔz (m^3)	4.63×10^{-6}
Total number of macroparticles in the simulation domain	2×10^{7}
Number of PIC cycles necessary to reach the convergence	10000
Adiabatic exponent γ	1.1
Reference electron density n_0 (m^{-3})	3×10^{13}
Reference electron temperature T_0 (eV)	1.5
Normalized impact parameter β_∞	15
Fitting parameter A (eV$^{-1/4}$)	2.5

III. Discussion of Results

The simulation takes 10000 time steps to reach a steady stage and 5000 time steps more for sampling. It takes 3 hours on a 8 Quad Core Intel Xenon X5570 (2.93 GHz, 96 GB RAM) cluster. The steady state is determined by the slow dynamics of CX ions, CX Xe^+ ions represent 7% of the total Xe^+ population, while CX Xe^{++} ions represent 14% of the total Xe^{++} ion population. In Fig. 5 the evolution of the number of macro-particles is reported.

Figs 6. show Xe^+ ion number density contours in planes Πx1, Πx2, Πz1 (z=0.1 m) and Πz2 (z=1 m), while Fig. 7.a shows Xe^+ ion number density y-profiles a different axial distance that lie on Πx1 and Fig. 7.b shows Xe^+ ion number density profile along three different axial lines that lie on Πx1: line centered between channel 1 and 4 ($x=L_x/2$, $y=(L_y+\Delta)/2$), centerline of the 4channel configuration ($x=L_x/2$, $y=L_y/2$) and line centered between channel 2 and 3 ($x=L_x/2$, $y=(L_y-\Delta)/2$). These figures indicate that the plumes from different channels merge into one already at a distance z=0.18 m from the multi-channel exit plane reaching a peak value of 2×10^{16} m^{-3}. Additional four peaks at z=0.14 m are evident from the axial profiles centered between two channels, result of the overlapping of the plume coming from two adiacent channels. The general shape formed by one central peak and four lateral peaks is still present 1 m from the exit plane (see the distribution in the Πz2 plane and Fig. 7.a). As Fig. 6.b shows, the maximum number density 3.5 cm downstream of the cluster exit plane is

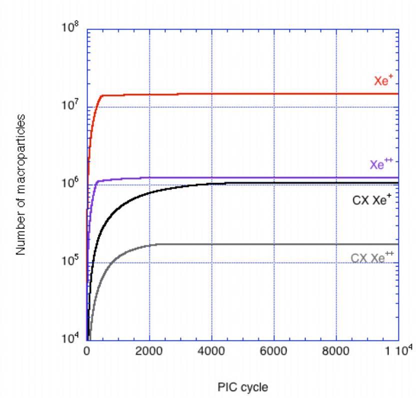

Figure 5. Evolution of the number of macroparticles during the simulation.

approximately 3.5x10^{17} m^{-3}, just as it is downstream of a single channel. The density falls off rapidly in the downstream direction and by z=15 cm the maximum plasma density has decreased by more than an order of

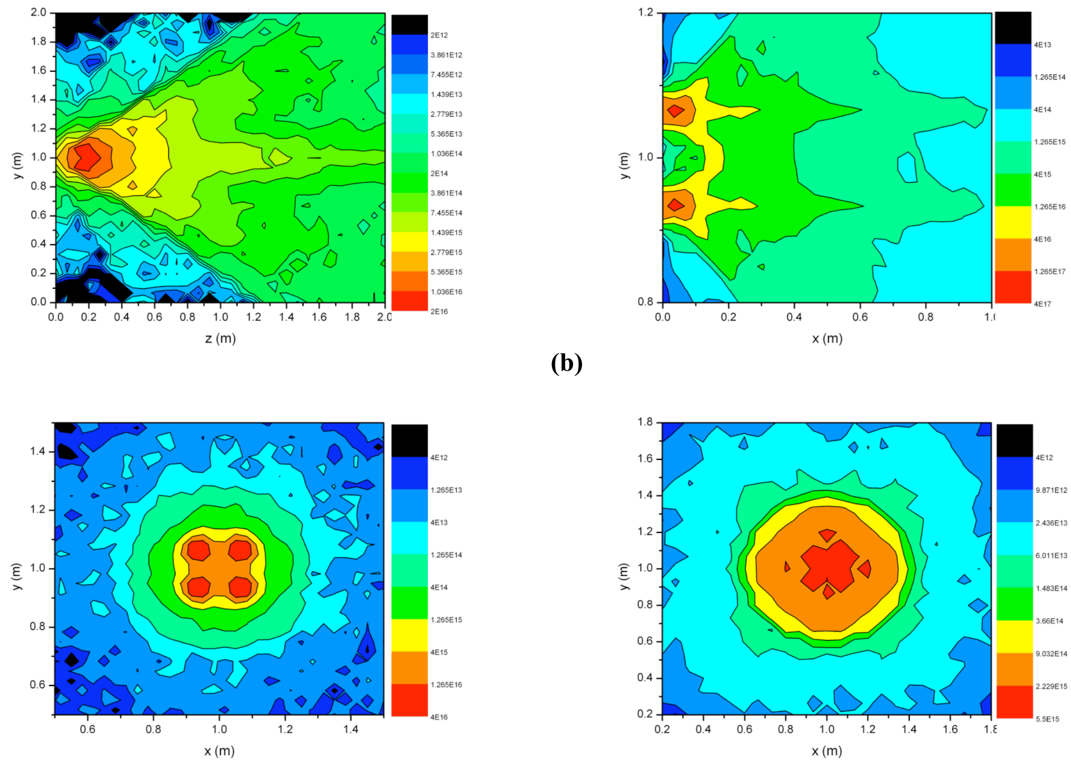

(a) (b) (c) (d)

Figure 6. Xe$^+$ ion number density (m^{-3}) contours in planes a) Πx1, b) Πx2, c) Πz1 and d) Πz2.

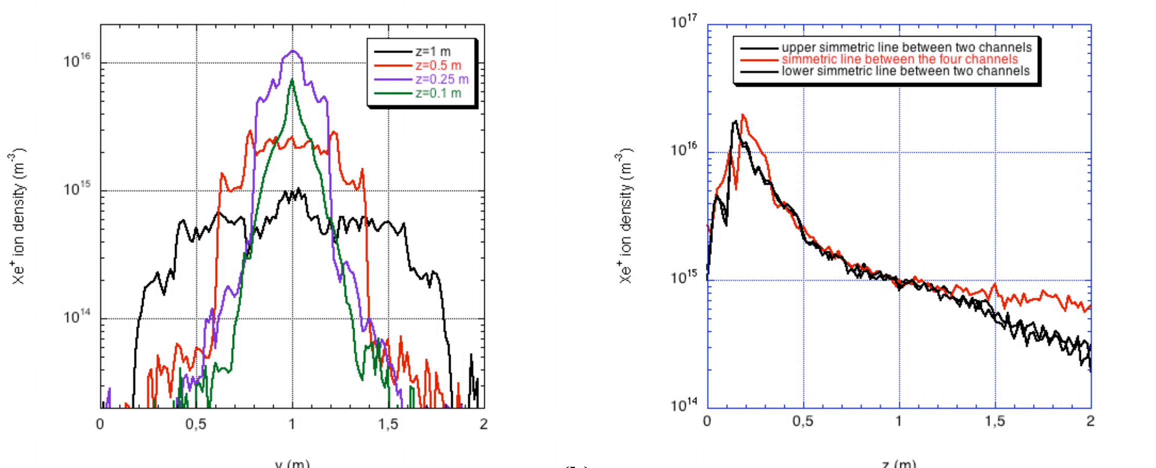

(a) (b)

Figure 7. Xe$^+$ ion number density (m^{-3}) a) y-profiles a different axial distance on plane Πx1 and b) z-profile along three different axial lines on plane Πx1.

magnitude to about 3x10^{16} m^{-3}. Fig. 6.b shows a well-defined jet structure downstream of each individual channel. By about 1 m downstream the plumes have merged to the point that the density is nearly constant across the width Δ of the configuration and resembles the profile that would be expected downstream of a large monolithic thruster.

Figs 8 show plasma potential contours in plane Πx1, Πx2, Πz1 (z=0.1 m) and Πz2 (z=1 m), while Fig. 9 shows plasma potential profiles along four different axial lines: axis line of channel 4, line centered between channel 3 and 4 (x=(L_x+Δ)/2, y=L_y/2), axis line of channel 3 and centerline of the overall configuration (x=L_x/2, y=L_y/2). As shown, the potential drops monotonically along the axis of each channel, while it reaches a peak of 14 V at an axial distance of 0.14 and 0.18 m along the symmetric line between channel 3 and 4 and along the centerline of the entire

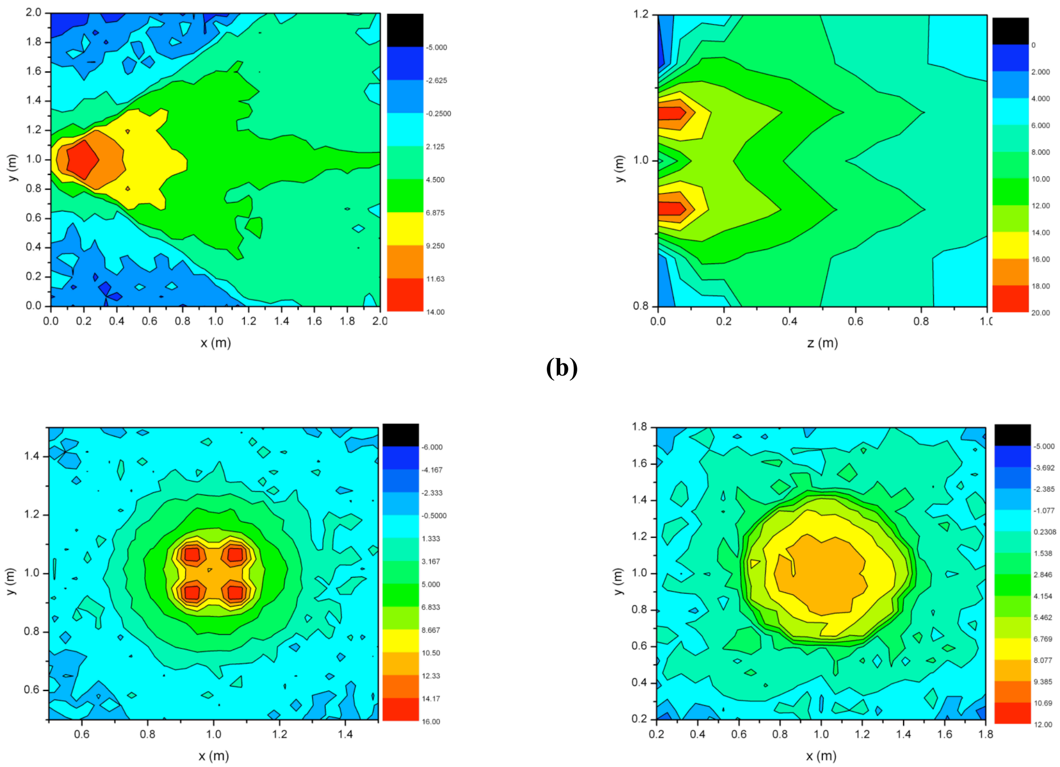

(a) **(b)**

(c) **(d)**

Figure 8. Plasma potential (V) contours in planes a) Πx1, b) Πx2, c) Πz1 and d) Πz2.

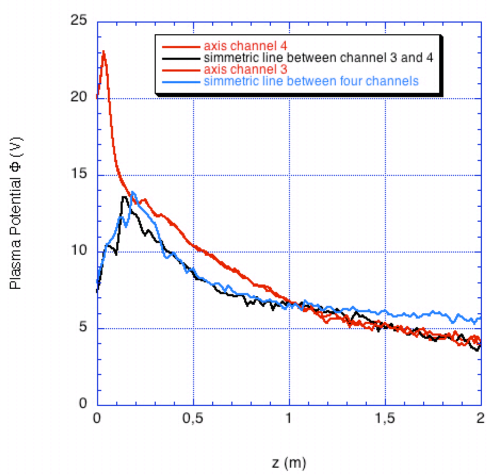

Figure 9. Plasma potential (V) profiles along four different axial lines.

configuration, respectively. These peaks correspond to peaks observed for the ion density. By 1 m downstream, the peak potential falls to less than 6 V. Moving radially away from the multichannel configuration, the plasma potential is seen to fall to approximately 6 V within about 0.1 m of the centerline of each channel. An interesting feature evident from Figs. 8.b, 8.c and 9 is the plasma potential behaviour in the area between the channels for z<0.20 m. There exists an electric potential well, that is the electric field vector is oriented in the upstream direction. The reversed electric field could potentially cause ions produced in the area between the channels as a result of CX collisions (the neutral density is maximum in this region due to the emission from the cathode neutralizer) to be accelerated upstream toward the surface of the configuration. Although this could hypothetically result in an increased erosion rate in some areas due to increased ion impingement, the effect will almost certainly be negligible in any practical situation since the impinging ions are unlikely to experience accelerating potentials greater than 5 V in the reverse direction.

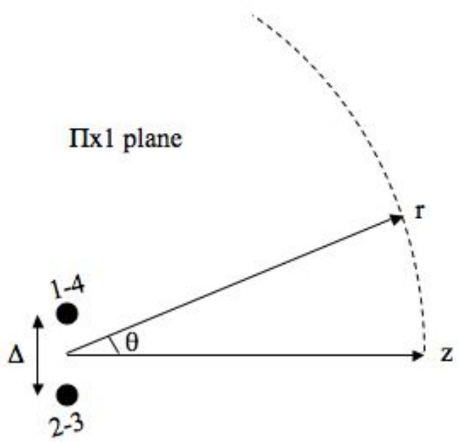

(a)

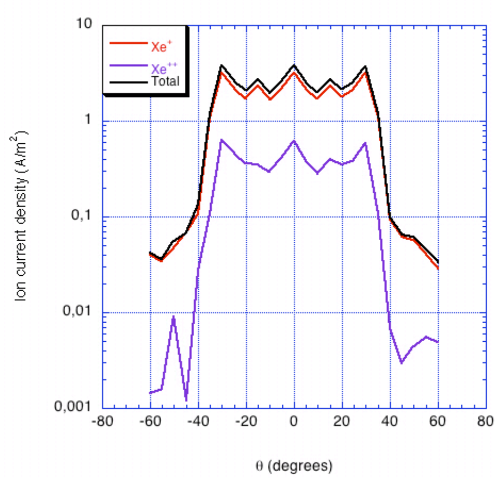

(b)

Figure 10. (a) Sketch of the location (r=1 m) where ion density current and ion energy distribution function have been detected. (b) Ion current density (A/m^2) detected at different angles.

Fig. 10.b shows Xe^+ and Xe^{++} ion current density (component parallel to the radial direction r) downstream of the configuration detected along a 1 m radial arc in the equatorial plane Πx1 (see Fig. 10.a). The "crown" shape characterized by one central peak at θ=0° and two secondary peaks at θ=±15° and θ=±30° is the result of the ion density y profile at different axial location (see Fig. 7.a, in particular black and red lines) coming from the interaction of the different plumes emitted from each channel.

Fig. 11.a shows the ion radial energy distribution function (IEDF) at a distance of 1 m from the center of the configuration for angle θ=0°. It is evident the presence of low energy CX ions far from the primary beam Xe^+ and Xe^{++} ions. Figs. 11.b show the fine structure of primary beam Xe^+ ions for different angles along the equatorial plane Πx1. A double peak is present for low angles and it is no more distinguishable for $|\theta|$>40°. The double peaked distribution is characterized by a convolution of a lower asymmetric Maxwell-Boltzmann distribution and a higher symmetric one. The most probable candidate for this IEDF shape seems to be a geometrical effect. In fact, as shown in Fig. 11.c, ions emitted in the external part of the dashed circle have to cross the dashed circle itself and then the peak of the potential represented by each beam before to reach a point in the equatorial plane. These paths make the ions to lose almost 20 eV before to reach the detection point in comparison to the ions emitted in the inner part of the circle. Previous numerical simulations claimed elastic scattering as responsible for the secondary lower peak in the ion energy spectra [17]. For this reason we have launched a case without elastic collisions and nevertheless the secondary peak is not disappeared.

Finally, Figs. 12 represent a snapshot in the space phase and in the velocity phase of Xe^+ ions (in red primary beam ions and in green CX ions) of the steady state.

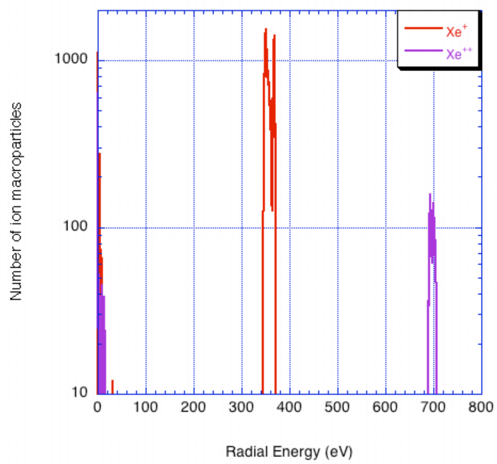

(a)

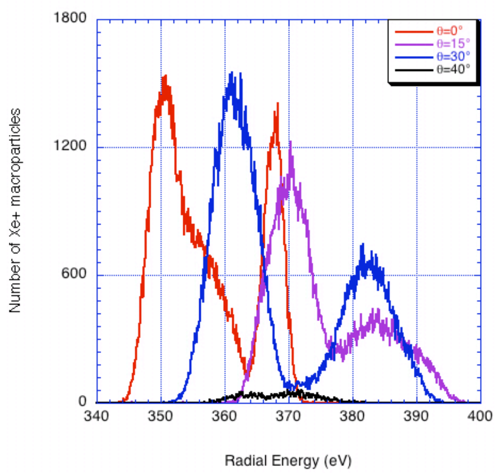

(b)

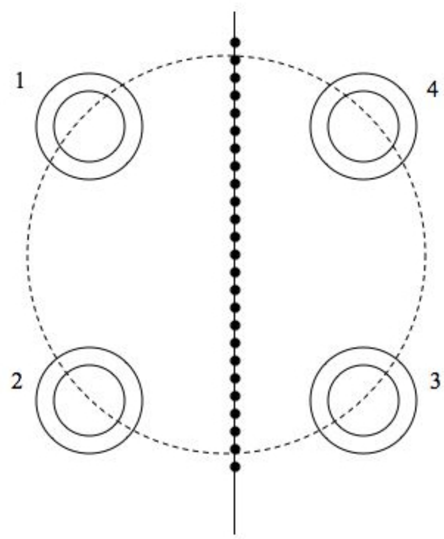

(c)

Figure 11. (a) Ion radial energy distribution function in the total energy range detected at θ=0. Ion radial energy distribution function of the primary beam Xe^{+} ions at different angles. Sketch explaining the geometrical effect causing the double peak structure in the ion energy spectra detected in the equatorial plane of the configuration.

IV. Conclusion

This work represents a three-dimensional model of the plume emitted from a four-channel SPT-40 configuration. The model consists of a hybrid (fluid electron and ion particle representation) Particle-in-Cell coupled with a Test-Particle Monte Carlo method for ion-neutral (momentum and charge exchange) collisions. The plume is characterized by the presence of a potential well in the central region for an axial distance smaller than 20 cm from the exit plane of the configuration. The most interesting result is the presence of a double peak in the ion energy spectrum that is due to a geometrical effect. Future works will concentrate on a better fluid electron representation, in particular in the very near-field plume region, where magnetic field and gradient effects are very important.

(a)

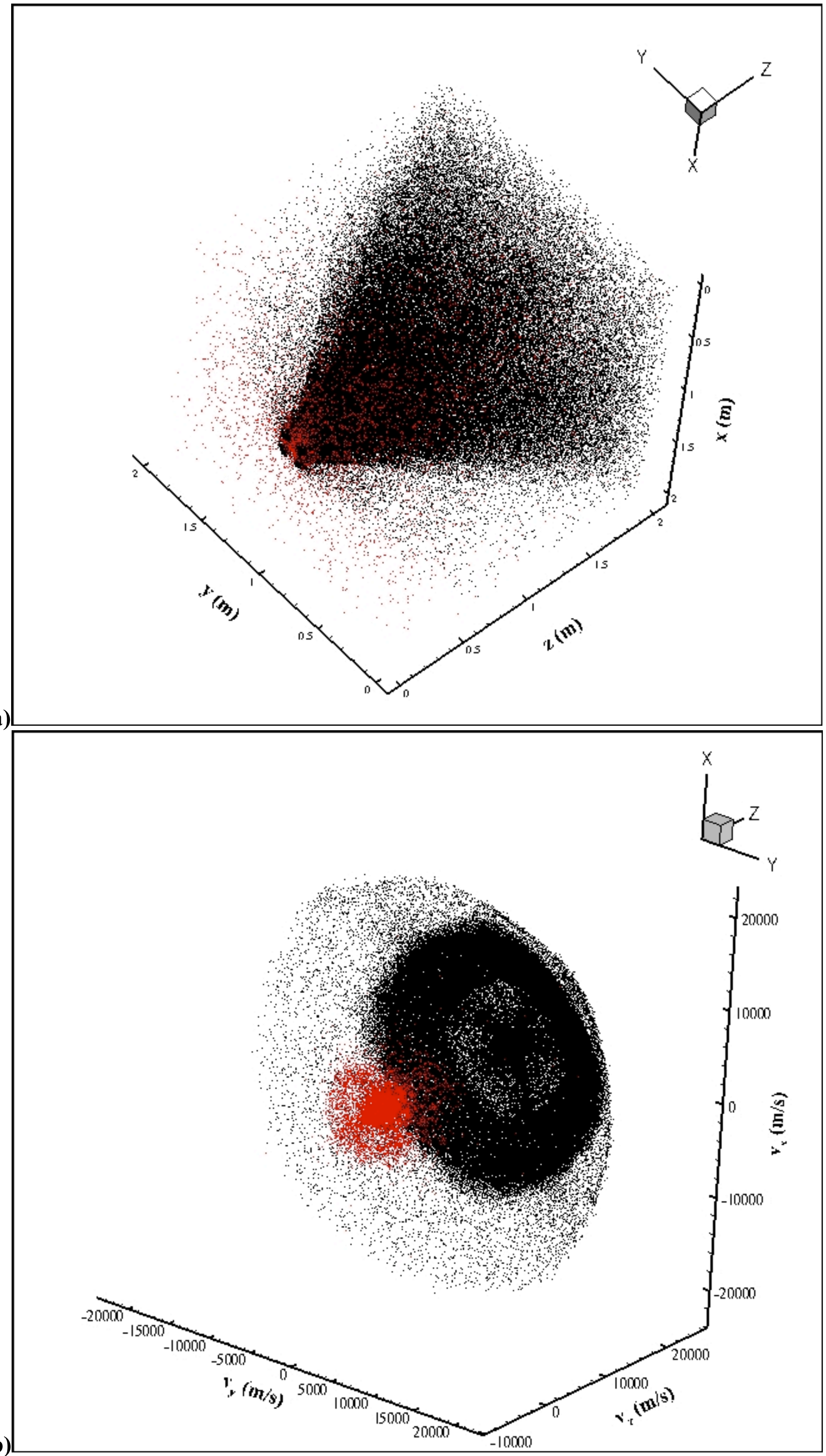

(b)

Figure 12. (a) Snapshot of Xe^+ ions (primary beam ions in black and CX ions in red) at the steady state (a) in the ordinary space phase and (b) in the velocity space phase.

Acknowledgments

This work has been supported by Ministero Sviluppo Economico under law 46/82 Project Number C01/0725/02/X06 and by CNR Progetto di Formazione Individuale – Dipartimento Materiali e Dispositivi, fase a regime 2008/2009.

References

[1]Jankovsky, R. S., et al., "50 kW Class Krypton Hall Thruster Performance", *AIAA-2003-4550*, 2003.

[2]Zakharenko, L. E., et al., "Study of Multi-Thruster Assembly Operation", *IEPC-03-311*, 2003.

[3]Beal, B. E., et al., "Plasma Properties in the Plume of a Hall Thruster Cluster", *J. Propulsion and Power*, Vol. 20, No. 6, 2004, pp. 985-991.

[4]Duchemin O., et al., "Multi-Channel Hall-Effect Thrusters: Missions Applications and Architecture Trade-Off", *IEPC-07-227*, 2007.

[5]Walker, M. L. R. Gallimore, A. D., "Hall Thruster Cluster Operation with a Shared Cathode", *J. Propulsion and Power*, Vol. 23, No. 3, 2007, pp. 528-536.

[6]Duchemin, O., Valentian, D., "Thrust Vector Control using Multi-Channel Hall-Effect Thrusters", *AIAA-2007-5203*, 2007.

[7]Roy. R. S., "Numerical Simulation of Ion Thruster Plume Back Flow for Spacecraft Contamination Assessment", Ph.D. thesis, Massachusetts Institute of Technology, 1995.

[8]VanGilder, D. B., "Numerical Simulation of The Plume of Electric Propulsion Thrusters", Ph.D. thesis, Cornell University, 2000.

[9]Eastwood, J. W., and Hockney, R. W., *Computer Simulation using Particle*, McGraw-Hill, New York, 1981.

[10]Birdsall, C. K., and Langdon, A. B., *Plasma Physics via Computer Simulation*, McGraw-Hill, New York, 1985.

[11]Taccogna, F., Longo, S., and Capitelli, M., "Particle-in-Cell with Test-Particle Monte Carlo (PIC/TPMC) Simulation of SPT-100 Exhaust Plumes," *J. Spac. & Rock.*, Vol. 39, No. 3, 2002, pp. 409-419.

[12]Taccogna, F., Longo, S., and Capitelli, M., "Very-near-field plume simulation of a stationary plasma thruster," *Europ. Phys. J., Appl. Phys.*, Vol. 28, 2004, pp. 113-122.

[13]Cai, C., "Theoretical and Numerical Studies of Plume Flows in Vacuum Chambers", Ph.D. thesis, University of Michigan, 2005.

[14]Bird, G. A., *Molecular gas dynamics and the direct simulation of gas flows*, Clarendon press, Oxford, 1994.

[15]Boccaletto, L., "Electric thruster technologies SPT-100 ion inflow data," Technical report No. WP-3 ESA/ESTEC 12736/97/NL/PA, December 1999.

[16]Nanbu, K., Kitatani, Y., "An ion-neutral species collision model for particle simulation of glow discharge", *J. Phys. D: Appl. Phys.*, Vol. 28, 1995, pp. 324-330.

[17]Katz, I., Jongeward, G., Davis, V., Mandell, M., Mikellides, I., Dressler, R., Boyd, I., Kannenberg, K., Pollard, J., and King, D., "A Hall Effect Thruster Plume Model Including Large-Angle Elastic Scattering," *AIAA-2001-3355*, 2001.